Particle-fluid simulation of the auroral current circuit

Jörgen Vedin and Kjell Rönnmark

Department of Physics, Umeå University, SE-901 87 Umeå, Sweden

Abstract. The incompatibility between stationary kinetic and dynamic fluid descriptions of auroral electron acceleration has been an outstanding problem in space physics for decades. In this study we introduce a new numerical simulation model that provides a unified picture by including electron temperature variations consistent with kinetic theory in the fluid description. We demonstrate that this new particle-fluid model can describe the partial reflection of Alfvén waves from the acceleration region, as well as the formation of a field-aligned potential drop proportional to the upward current. Simulations based on the particle-fluid concept can be applied to various processes in space physics and astrophysics where strong currents flowing along an inhomogeneous magnetic field will cause temperature increases and field-aligned electric fields.

1. Introduction

Numerical simulations are important tools in studies of space plasma physics. Particle-In-Cell (PIC) models can often successfully be applied also when most other methods fail, for example when describing nonlinear kinetic processes involving strong turbulence and particle trapping in large amplitude waves. However, the use of PIC codes is restricted to rather fast and small scale phenomena. For stability reasons we must in a PIC code use a time step Δt comparable to the inverse plasma frequency ω_p^{-1} and a spatial resolution $\Delta z \sim \lambda_D$, where λ_D is the Debye length. In the inhomogeneous magnetospheric plasma, these constraints make PIC simulations of global processes on time scales of several minutes impractical.

Fluid models provide reduced descriptions of the plasma, and their flexibility allows unwanted high frequency modes to be removed. The restrictions on Δt and Δz can then be relaxed, and this makes fluid models more suitable for global simulations. The drawback is that fluid models fail to describe some kinetic processes, which sometimes can be important also in global simulations. Usually, the hierarchy of fluid equations is closed by assuming an equation of state, but in the presence of large flows along an inhomogeneous magnetic field in a collisionless plasma there is no simple relation between the local density and temperature variations [*Ramos*, 2003; *Vedin and Rönnmark*, 2005]. This indicates that the relevant physics cannot properly be described by a fluid model based on a local equation of state. An important case where fluid models are inadequate is the acceleration of auroral electrons, and similar processes may also be common in various astrophysical contexts.

In this study we present a new type of simulation model that may be used when neither PIC nor fluid models are appropriate. The algorithm is in principle similar to a PIC code, but in addition to Maxwell's equations we include the fluid continuity and momentum equations in the field solver. The only unknown variables in the field solver are then the parallel and perpendicular temperatures, which are provided by the particles. Since the field solver does not use the particle charge density or current, we can in the particle pusher reduce the interaction between the particles without affecting the simulated fields. This allows us to reduce the effective plasma frequency of the particles and increase the effective Debye length. Since this can be done without modifying the velocity scale ($\propto \omega_p \lambda_D$), the reduction of the electrostatic force between particles will not affect the temperatures derived from the particle distribution. The detailed model description is given in section 2, but first we will explain why this particle-fluid approach is needed in studies of auroral electron acceleration.

Electrons that are accelerated along the Earth's magnetic field lines can create discrete auroras when they precipitate into the ionosphere. Fluid simulations are an important tool in studies of processes related to electron acceleration in the auroral current circuit, since the magnetosphere-ionosphere coupling that drives the current is characterized by relatively long time scales (seconds to minutes) and large length scales (several R_E). However, collisionless fluid simulations have not been able to reproduce the large field-aligned electric fields that are observed [e.g., *Hoffman*, 1993; *Evans*, 1968, 1974; *Mizera and Fennel*, 1977] as well as predicted by kinetic theory [e.g., *Knight*, 1973; *Chiu and Schulz*, 1978].

Let us consider the effect such a field-aligned electric field would have on the auroral electrons. When the electric field accelerates the electrons down the converging magnetic field lines, the mirror force converts much of the field-aligned velocity into perpendicular velocity. This effect, together with the loss cone, leads to a horseshoe shaped velocity distribution with much higher temperatures in the acceleration region than above. The electric field is then self-consistently sustained by electron pressure gradients. This has been neglected in previous fluid models by assuming cold [*Lysak and Dum*, 1983; *Lysak*, 1985; *Kletzing*, 1994] or isothermal [*Goertz and Boswell*, 1979; *Streltsov et al.*, 1998; *Rönnmark and Hamrin*, 2000; *Streltsov and Lotko*, 2003] electrons. On the other hand, most PIC or hybrid simulations of auroral electrons [*Hui and Seyler*, 1992; *Damiano et al.*, 2003; *Génot et al.*, 2000, 2001] have not been able to describe the temperature increase since the background magnetic field has been assumed homogeneous. The electrostatic PIC simulations of *Schriver* [1999] included an inhomogeneous magnetic field, but electron temperature increases caused by steady currents were not considered. Only recently the importance of electron temperature variations has been emphasized in some observational [*Hull et al.*, 2003a, b] as well as theoretical [*Vedin and Rönnmark*, 2004, 2005] studies.

To include temperature variations in a fluid model we need an equation of state applicable to the auroral electrons. However, when a field-aligned electric field accelerates the electrons, the temperature increase is not localised to the acceleration region. Since the electron motion along the field lines is collisionless, the temperatures are affected all along

0148-0227/06/$9.00

the field line. Due to this nonlocal effect we cannot, as in collision-dominated plasmas, use a local equation of state to close the set of fluid equations [*Vedin and Rönnmark*, 2005]. Instead, we need to complement the fluid description by treating the electrons as individual particles. This can be accomplished by using the particle-fluid model presented in this paper.

In our model the dynamics is driven by a generator near the equatorial plane. The generator is here implemented as a volume force, in contrast to previous models [e.g., *Lysak*, 1985] where it is implemented as a boundary condition. We first use a generator that causes a transition from a current free state to a quasi-stationary state with a significant steady current. With this type of generator we can study the current-voltage relation and the evolution of the electromagnetic fields and the electron distribution during the build-up of a discrete auroral arc. We will also use a second form of the generator, which drives monochromatic shear Alfvén waves along the field line. This allows us to investigate the reflection of Alfvén waves and field line resonances, which have been the object of numerous studies [*Cheng et al.*, 1993; *Streltsov et al.*, 1998; *Streltsov and Lotko*, 1999; *Tikhonchuk and Rankin*, 2000]. The monochromatic generator model is more relevant to auroras in the Alfvénic region near the polar cap boundary of the auroral zone [e.g., *Paschmann et al.*, 2002, Ch. 4], but in this study we are not aiming to describe a particular type of aurora in detail.

Our intent in this paper is to focus on the introduction of the new particle-fluid simulation model, rather than on the presentation of new results. Therefore, the next section contains an extensive description of the theory behind the model and the algorithm handling the coupling between the field solver and the particles. Section 3 presents some first results to show that the model is working properly and to indicate which types of processes that can be studied with the model. Finally, in section 4 we discuss the implications of the model and draw some conclusions.

2. Theory and Simulation Model

The geometry of the auroral current circuit and the generator region in the equatorial magnetosphere is sketched in Figure 1. We introduce a coordinate system based on the flux tube geometry, with z along the magnetic field lines, x increasing to the earth and y to the west. The origin of this coordinate system is at a point where an auroral field line crosses the equatorial plane. Since x and y are constant along the converging field lines, a distance dl is related to these coordinates by the metric

$$dl^2 = (dx^2 + dy^2)\frac{B_M}{B_z} + dz^2, \tag{1}$$

where $B_z(z)$ is the geomagnetic field and B_M is the field strength at $z = 0$ in the equatorial plane. We neglect the curvature of the field lines, and assume homogeneity in the y direction.

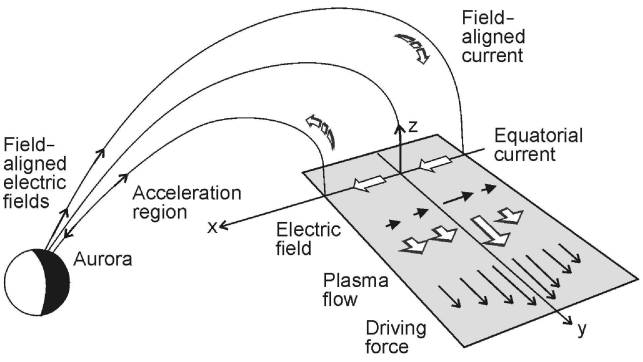

Figure 1. The geometry of the auroral current circuit and the generator region in the equatorial magnetosphere. The curvature of the magnetic field lines is neglected in our model equations.

2.1. Maxwell's Equations

The current density $\mathbf{j} = j_x\hat{\mathbf{x}} + j_z\hat{\mathbf{z}}$ will according to Maxwell's equations couple to the electric field components E_x, E_z, and the magnetic field B_y. Ampere's and Faraday's laws for these fields are in our coordinate system expressed as

$$\partial_t E_x = -c^2\left(\partial_z B_y - B_y\frac{\partial_z B_z}{2B_z} + \mu_0 j_x\right), \tag{2}$$

$$\partial_t E_z = c^2\left(\sqrt{\frac{B_z}{B_M}}\,\partial_x B_y - \mu_0 j_z\right), \tag{3}$$

$$\partial_t B_y = \sqrt{\frac{B_z}{B_M}}\,\partial_x E_z - \partial_z E_x + E_x\frac{\partial_z B_z}{2B_z}, \tag{4}$$

where $c = (\varepsilon_0\mu_0)^{-1/2}$ is the speed of light.

The ion motion along the field lines is neglected, and we assume that the ion velocity U_y in the y direction is given by the $\mathbf{E}\times\mathbf{B}$ drift. We will consider the ions to be cold, which implies that the ion kinetic effects on Alfvén wave propagation are neglected, although they may be significant at altitudes above a few R_E. Including a prescribed mechanical force F_y that drives the generator, the y component of the equation of motion for the ions is

$$d_t U_y = -\frac{e}{m_i}U_x B_z + \frac{F_y}{n_i m_i}, \tag{5}$$

where e is the proton charge, n_i is the ion density, and m_i is the ion mass. Using $U_y = -E_x/B_z$ in this equation allows us to calculate the ion velocity U_x and the current j_x, which essentially is the ion polarization current. Inserting this current in Ampere's law gives [*Rönnmark and Hamrin*, 2000]

$$\partial_t E_x = -\mathsf{A}^2 c^2\left(\partial_z B_y - B_y\frac{\partial_z B_z}{2B_z}\right) - (1-\mathsf{A}^2)\frac{B_z}{n_i m_i}F_y, \tag{6}$$

where

$$\mathsf{A}^2 = V_A^2\frac{1 - \frac{m_i}{eB_z^2}\sqrt{\frac{B_z}{B_M}}\,\partial_x E_x}{c^2 + V_A^2\left(1 - \frac{m_i}{eB_z^2}\sqrt{\frac{B_z}{B_M}}\,\partial_x E_x\right)},$$

and $V_A = B_z/\sqrt{\mu_0 n_i m_i}$ is the Alfvén velocity.

2.2. Fluid Equations

The evolution of the phase space density f is determined by the Vlasov equation

$$d_t f = \partial_t f + \mathbf{v}\cdot\nabla f - \frac{e}{m}\left(\mathbf{E} + \mathbf{v}\times\mathbf{B}\right)\cdot\partial_{\mathbf{v}} f = 0, \tag{7}$$

where m is the electron mass. We consider one spatial dimension z and two velocity dimensions $v_z = \dot{z}$ and $v_\perp$ implying that the phase space density is a function of only four variables, $f = f(v_z, v_\perp, z, t)$, and the Vlasov equation can

be rewritten as

$$\partial_t f + v_z \partial_z f - \left(\frac{eE_z}{m} + \frac{v_\perp^2 \partial_z B_z}{2B_z} \right) \partial_{v_z} f + \frac{v_\perp v_z \partial_z B_z}{2B_z} \partial_{v_\perp} f = 0. \quad (8)$$

When the phase space density f is known, we can calculate fluid quantities such as the electron density

$$n = \int f \, d\mathbf{v}, \quad (9)$$

the field-aligned bulk flow velocity

$$u_z = \frac{1}{n} \int v_z \, f \, d\mathbf{v}, \quad (10)$$

the parallel temperature

$$T_z = \frac{1}{n} \int m(v_z - u_z)^2 \, f \, d\mathbf{v}, \quad (11)$$

and the perpendicular temperature

$$T_\perp = \frac{1}{n} \int \frac{m v_\perp^2}{2} \, f \, d\mathbf{v}. \quad (12)$$

From these definitions we can also construct the field-aligned current density $j_z = -enu_z$. Taking moments of equation (8) we can derive the fluid equations relating the above defined fluid quantities to each other. Integrating the Vlasov equation over velocity space we find the continuity equation for electrons

$$\partial_t n = -\partial_z (n u_z) + n u_z \frac{\partial_z B_z}{B_z} \, . \quad (13)$$

Multiplying the Vlasov equation by ev_z before integrating over velocity space we find the momentum equation

$$\begin{aligned} \partial_t j_z &= \frac{e^2 n}{m} E_z + \partial_z \left(\frac{e}{m} n T_z + \frac{j_z^2}{en} \right) \\ &- \left(\frac{e}{m} (n T_z - n T_\perp) + \frac{j_z^2}{en} \right) \frac{\partial_z B_z}{B_z} \, . \end{aligned} \quad (14)$$

To determine the temperatures that are needed in the momentum equation we can either use the next level in hierarchy of fluid equations, i.e. the energy equations, or some equation of state. If the energy equations are used the problem of closing the hierarchy of fluid equations is just moved to the next level, and we then need to determine the heat conduction. If an equation of state is to be used, we need to find such an equation applicable to auroral electrons, but, as discussed in *Vedin and Rönnmark* [2005], this is a difficult task as the temperatures at one position along the field line depend on the history and present state of the entire auroral flux tube.

2.3. Field Solver

We now introduce new dimensionless independent variables through

$$\mathsf{x} = \tfrac{\Omega_i}{c} x, \;\; \mathsf{z} = \tfrac{\Omega_i}{c} z, \;\; \mathsf{t} = \Omega_i t, \quad (15)$$

where $\Omega_i = eB_M/m_i$, and the dimensionless fields

$$\begin{aligned} \mathsf{E_x} &= E_x / \sqrt{c^2 B_M B_z} \, , \\ \mathsf{E_z} &= E_z / (c B_M) \, , \\ \mathsf{B} &= B_y / \sqrt{B_M B_z} \, , \\ \mathsf{n} &= n m_i / (\varepsilon_0 B_M B_z) \, , \\ \mathsf{j} &= \mathsf{n} \frac{u_z}{c} = -\frac{\mu_0 c}{\Omega_i B_z} j_z \, , \\ \mathsf{T} &= T / (mc^2) \, , \\ \mathsf{F} &= \frac{F_y}{n_i m_i c \, \Omega_i \sqrt{B_M / B_z}} \, . \end{aligned} \quad (16)$$

The governing equations (6), (3)-(4), (13)-(14) can then be rewritten in these dimensionless simulation variables as

$$\partial_\mathsf{t} \mathsf{E_x} = -\mathsf{A}^2 \partial_\mathsf{z} \mathsf{B} - (1 - \mathsf{A}^2) \mathsf{F} \, , \quad (17a)$$

$$\partial_\mathsf{t} \mathsf{E_z} = \frac{B_z}{B_M} (\partial_\mathsf{x} \mathsf{B} + \mathsf{j}) \, , \quad (17b)$$

$$\partial_\mathsf{t} \mathsf{B} = \partial_\mathsf{x} \mathsf{E_z} - \partial_\mathsf{z} \mathsf{E_x} \, , \quad (17c)$$

$$\partial_\mathsf{t} \mathsf{n} = -\partial_\mathsf{z} \mathsf{j} \, , \quad (17d)$$

$$\partial_\mathsf{t} \, \mathsf{j} = -\frac{m_i}{m} \mathsf{n} \mathsf{E_z} - \partial_\mathsf{z} \left(\mathsf{n} \mathsf{T_z} + \frac{\mathsf{j}^2}{\mathsf{n}} \right) - \mathsf{n} \mathsf{T}_\perp \frac{\partial_z B_z}{B_z} \, . \quad (17e)$$

These equations describe the propagation of shear Alfvén waves but also high-frequency waves such as electrostatic oscillations at the plasma frequency ω_p and electromagnetic radiation with the phase velocity c. To numerically integrate these equations with an explicit algorithm we need to fulfill the stability conditions $\Delta t < (\omega_p / 2\pi)^{-1}$ and $\Delta t < \Delta x / c$, where Δx is the perpendicular resolution. By using an implicit time stepper we can obtain a stable solution without fulfilling these stability conditions, but to obtain a reasonably accurate solution we still need to keep the time step relatively close to these conditions. This implies that with typical plasma parameters we would need to use a time step of $\Delta t \sim 10^{-5}$ s, while the interesting physical processes related to the Alfvén waves have time scales of ~ 1 s. In related numerical models [e.g., *Goertz and Boswell*, 1979; *Lysak and Dum*, 1983; *Streltsov and Lotko*, 1999] this problem is handled by neglecting the parallel displacement current $\varepsilon_0 \partial_t E_z$. In some recent studies [*Rönnmark and Hamrin*, 2000; *Lysak and Song*, 2001; *Vedin and Rönnmark*, 2005] the parallel displacement current has been included and the problem with the numerical integration has been handled by introducing an anisotropic vacuum.

The anisotropy is introduced if we in Ampere's law replace ε_0 by a dielectric tensor

$$\varepsilon_0 \begin{pmatrix} 1 & 0 & 0 \\ 0 & 1 & 0 \\ 0 & 0 & \varepsilon_z \end{pmatrix} \, , \quad (18)$$

where $\varepsilon_z = 1$ in normal vacuum. Equation (17b) then becomes

$$\partial_\mathsf{t} \mathsf{E_z} = \frac{B_z}{\varepsilon_z B_M} (\partial_\mathsf{x} \mathsf{B} + \mathsf{j}) \, . \quad (19)$$

This also implies that the plasma frequency and the phase velocity of the ordinary electromagnetic mode are rescaled as $\omega_p^* = \omega_p / \sqrt{\varepsilon_z}$ and $c^* = c / \sqrt{\varepsilon_z}$, but it still leaves the electron inertial length $\lambda_e = c / \omega_p$ unchanged. Thus, by increasing ε_z we can slow down the fastest processes described by equations (17) without changing the important scale length λ_e. If we choose

$$\varepsilon_z = \max[(\omega_p \Delta t)^2, 1] \, , \quad (20)$$

we can resolve plasma oscillations whenever $\omega_p \Delta t < 1$, but otherwise the plasma frequency is reduced to $\omega_p^* = \Delta t^{-1}$,

which can be handled by the numerical integration. The time step used here is still such that the effective plasma frequency ω_p^* is much greater than the frequencies of interest, and the difference between ω_p^* and ω_p does therefore not affect the results.

For a more comprehensive discussion about the anisotropic vacuum and the physical processes described by equations (17) we refer to *Rönnmark and Hamrin* [2000]. They also describe the details in the implicit Crank-Nicholson algorithm used in the numerical integration.

2.4. Computing the temperatures

To close the set of fluid equations (17) in the field solver, we calculate the temperatures from a simulation of the electron motion along the field lines. The algorithm is self-consistent in the same sense as other PIC codes. We accelerate the particles by the electric field from the field solver, and from the velocity distribution of the electrons we can from equations (11) and (12) determine temperatures that can be used in the momentum equation.

Since the auroral electrons are strongly magnetized their displacement in the x direction is negligible, and their perpendicular velocity can be determined from the conserved magnetic moment

$$\mu = \frac{m v_\perp^2}{2B_z} \,. \tag{21}$$

Along a field line, the position and velocity of a particle are updated according to the equations of motion

$$d_t z = v_z \,, \tag{22}$$

$$d_t v_z = -\frac{1}{m}\left(eE_p + \mu \partial_z B_z\right) \,, \tag{23}$$

where E_p is the electric field that accelerates the particle. The electric field E_p is mainly the electric field E_z from the field solver, but a correction is needed to keep the density and current of the particles equal to the density and current of the fluid.

To ensure that the current of the particles is equal to the current in the electron fluid, we notice that the evolution of an electric field $\mathsf{E_p}$ consistent with the particle current $\mathsf{j_p}$ is given by

$$\partial_\mathsf{t}\mathsf{E_p} = \frac{B_z}{\varepsilon_z B_M}\left(\partial_\mathsf{x}\mathsf{B} + \mathsf{j_p}\right) \,. \tag{24}$$

Subtracting equation (19) and introducing $\delta\mathsf{E} = \mathsf{E_p} - \mathsf{E_z}$ we find

$$\partial_\mathsf{t}\delta\mathsf{E} = \frac{B_z}{\varepsilon_z B_M}\left(\mathsf{j_p} - \mathsf{j}\right) \,. \tag{25}$$

Applying the correction $\delta\mathsf{E}$ would ensure that $\mathsf{j_p}$ closely follows j throughout the simulation. However, time integration of Ampere's law and the continuity equation may lead to accumulation of numerical errors, and cause growing inconsistencies between the charge density and the electrostatic field. To ensure that the the electric field and particle density remain consistent we derive part of the correction from Gauss' law in one dimension. Using the continuity equation $\partial_\mathsf{t}(\mathsf{n} - \mathsf{n_p}) = \partial_\mathsf{z}(\mathsf{j_p} - \mathsf{j})$, we rewrite equation (25) as

$$\partial_\mathsf{t}\delta\mathsf{E} = \frac{B_z}{\varepsilon_z B_M}\left[\theta\left(\mathsf{j_p} - \mathsf{j}\right) + (1-\theta)\partial_\mathsf{t}\int_0^\mathsf{z}\left(\mathsf{n} - \mathsf{n_p}\right)\mathsf{dz}'\right] \,, \tag{26}$$

where θ is a constant, $0 \le \theta \le 1$. Assuming that initially $\delta\mathsf{E} = 0$ and integrating over a time step Δt we obtain

$$\delta\mathsf{E} = \theta\,\delta\mathsf{E_A} + (1-\theta)\,\delta\mathsf{E_G} \,, \tag{27}$$

where

$$\delta\mathsf{E_A} = \Delta\mathsf{t}\frac{B_z}{\varepsilon_z B_M}\left(\mathsf{j_p} - \mathsf{j}\right) \,, \tag{28}$$

derived from Ampere's law, ensures that $\mathsf{j_p} \approx \mathsf{j}$ throughout the simulation, and

$$\delta\mathsf{E_G} = \frac{B_z}{\varepsilon_z B_M}\int_0^\mathsf{z}\left(\mathsf{n} - \mathsf{n_p}\right)\mathsf{dz}' + \frac{\sigma_0}{\varepsilon_\mathsf{z}} \,, \tag{29}$$

derived from Gauss' law ensures that $\mathsf{n_p} \approx \mathsf{n}$. The constant of integration σ_0 is determined by requiring

$$\int \delta\mathsf{E_G}\,\mathsf{dz} = 0 \,, \tag{30}$$

which ensures that $\delta\mathsf{E_G}$ does not produce a net potential drop and minimizes its effect on the current. A correction similar to $\delta\mathsf{E_G}$ is common in electromagnetic PIC codes. The parameter θ is in the code set to $\theta = 1/2$ which gives relatively weak trends and fluctuations in both $\mathsf{j_p} - \mathsf{j}$ and $\mathsf{n_p} - \mathsf{n}$. The value of θ is not crucial as long as it is not chosen close to 0 or 1. The particle current $\mathsf{j_p}$ will not follow the variations of j if θ is too small, and if $\theta \approx 1$ the density of the particles can deviate substantially from the corresponding values in the fluid after some time.

The particles are stepped forward in time using a leap-frog algorithm similar to that described by *Birdsall and Langdon* [1985] for an electromagnetic PIC code. Using the notation $\mathsf{f}^n \equiv \mathsf{f}(t^n) = \mathsf{f}(n\Delta t)$, the detailed algorithm that describes the coupling between the electric field $\mathsf{E_z}$ in the field solver and the particle simulation returning $\mathsf{n_p}$, $\mathsf{j_p}$, $\mathsf{T_z}$, and $\mathsf{T}_\perp$ can be written

$$\delta\mathsf{E_A}^n = \Delta\mathsf{t}\frac{B_z}{\varepsilon_z B_M}(\mathsf{j_p}^{n-\frac{1}{2}} - \mathsf{j}^{n-\frac{1}{2}}) \tag{31a}$$

$$\delta\mathsf{E_G}^n = \frac{B_z}{\varepsilon_z B_M}\int_0^\mathsf{z}(\mathsf{n}^n - \mathsf{n_p}^n)\,\mathsf{dz}' + \frac{\sigma_0^n}{\varepsilon_z} \tag{31b}$$

$$\mathsf{E_p}^n = \mathsf{E_z}^n + \theta\,\delta\mathsf{E_A}^n + (1-\theta)\,\delta\mathsf{E_G}^n \tag{31c}$$

$$\mathsf{a_z}^n = -\tilde{\mu}\partial_\mathsf{z}B_z(z^n) - \frac{m_i}{m}\mathsf{E_p}^n(z^n) \tag{31d}$$

$$\mathsf{v_z}^{n+\frac{1}{2}} = \mathsf{v_z}^{n-\frac{1}{2}} + \Delta\mathsf{t}\,\mathsf{a_z}^n \tag{31e}$$

$$\text{Compute } \mathsf{j_p}^-, \mathsf{T_z}^-, \mathsf{T}_\perp{}^- \text{ at } \mathsf{v_z}^{n+\frac{1}{2}}, \mathsf{z}^n \tag{31f}$$

$$\mathsf{z}^{n+1} = \mathsf{z}^n + \Delta\mathsf{t}\mathsf{v_z}^{n+\frac{1}{2}} \tag{31g}$$

$$\text{Compute } \mathsf{n_p}^{n+1}, \mathsf{j_p}^+, \mathsf{T_z}^+, \mathsf{T}_\perp{}^+ \text{ at } \mathsf{v_z}^{n+\frac{1}{2}}, \mathsf{z}^{n+1} \tag{31h}$$

$$\text{Compute } \mathsf{f}^{n+\frac{1}{2}} = \frac{1}{2}(\mathsf{f}^- + \mathsf{f}^+) \text{ where } \mathsf{f} = \mathsf{j_p}, \mathsf{T_z}, \mathsf{T}_\perp \tag{31i}$$

These equations are written in simulation variables, where we have renormalized the magnetic moment as $\tilde{\mu} = \mu/(mc^2)$. To calculate the moments of the particles and to compute the fields at the particle positions we use linear weights, i.e., a cloud-in-cell model. Note that the temperatures are calculated at $t^{n+1/2}$, which means that they are correctly included in the Crank-Nicholson algorithm used to solve the fluid equations.

The algorithm described above can be regarded as the second level in a hierarchy of increasingly fluid-like simulation models. Electrostatic PIC codes, where the particle density is used to solve Poisson's equation for the electric field, are on the zeroth level of this hierarchy since the field solver uses the zeroth moment of the particle distribution. In electromagnetic PIC codes the particle current is the source term in a field solver based on Ampere's law, Faraday's law, and at least implicitly the continuity equation. Such codes, which use the first moment of the particle distribution to solve for the fields, are on the first level. In the particle-fluid model described here the particle temperatures are fed to a field solver that includes the continuity and momentum equations. Since the fields are determined from the second moments of the particle distribution, this is a second level

model. Most high-frequency phenomena, including electrostatic and electromagnetic waves, are in this type of second level model handled within the field solver. Using an implicit field solver, we need not resolve these high frequencies. We can then use a time step suitable for the slow processes related to the build-up of auroral currents by Alfvén waves.

2.5. Model Parameters

All results presented in this study are based on a single set of model parameters. The simulation plane has the dimensions $0 < z < L_z$, $-L_x < x < L_x$, where $L_z = 5.5 \cdot 10^4$ km (or $8.6\,\mathrm{R_E}$) and L_x is 2000 km at the generator and 78.6 km in the ionosphere due to the convergent magnetic field lines. When presenting the results we will also use the height $h = L_z - z$ above the ionospheric boundary.

We use an inhomogeneous grid where Δz decreases with z and Δx is shortest near $x = 0$. This improves the resolution in the acceleration region and below, and it also resolves the details in the center region near $x = 0$ where the generator force is large. We use $nz = 100$ grid points in the z-direction and $nx = 27$ grid points in the x-direction. The resolution in the z-direction then varies between $\Delta z \approx 40$ km in the ionosphere and $\Delta z \approx 2200$ km at the generator boundary. In the acceleration region this implies a grid spacing of $\Delta z \approx 250$ km. In the ionosphere the x-resolution varies between $\Delta x \approx 3$ km near $x = 0$ and $\Delta x \approx 15$ km at the outer boundaries.

Since we use an implicit time stepper and increase ε_z as described by equation (20), the choice of time step Δt is not crucial for the field solver. We only need to make sure that $\omega_p^* = \Delta t^{-1}$ is much larger than the frequencies of interest (~ 1 Hz). However, the choice of Δt is important for the particle pusher. The basic stability criterion is that $v_{th}\Delta t < \Delta z$, where v_{th} is the electron thermal velocity. If $v_{th}\Delta t \lesssim \Delta z/\pi$ a nonphysical instability caused by the grid can occur [*Birdsall and Langdon*, 1985], but this instability is relatively mild and disappears when the time step is reduced even further ($v_{th}\Delta t \ll \Delta z/10$). It is thus not too difficult to avoid instabilities when choosing the time step, although we have two groups of electrons with very different thermal velocities in the system. The inhomogeneous grid also makes the choice of time step easier, since Δz is shortest where the ionospheric electrons with small thermal velocities dominate. In results presented here we have chosen $\Delta t = 0.02$ s.

The geomagnetic field strength is modeled by

$$\begin{aligned} B_z(z) &= B_M \exp[(z/L_z)^2(\ln(B_I/B_M) \\ &- 0.6 - 1.8(z/L_z)^2 + 2.4(z/L_z)^6)], \end{aligned} \tag{32}$$

with an ionospheric field strength $B_I = 56\ \mu$T and $B_M = 0.0864\ \mu$T. This magnetic field model approximates the dipole field for the $L = 7$ shell.

As mentioned in the introduction we will present results using two different generator models. When studying the transition from a current-free state to a quasi-stationary state we will use a force of the form

$$F_y(x,z,t) = F_0\ \exp\left(-\frac{z^2}{L_{zG}^2} - \frac{x^2}{L_{xG}^2}\right)\ \frac{t^2}{t^2 + t_G^2}\,, \tag{33}$$

to build up a steady current. Here, $F_0 = 1.0 \cdot 10^{-17}$ N m^{-3}, $L_{zG} = 6000$ km, $L_{xG} = 200$ km, and $t_G = 10$ s. The parameter L_{xG} controls the transverse scale of the driven Alfvén waves. It scales to about 8 km in the ionosphere, and about four times the electron inertial length in the acceleration region. The characteristic time t_G is the time it takes the generator force to reach half its final value.

When driving monochromatic Alfvén waves along the field lines we will use the force

$$F_y(x,z,t) = \begin{cases} F_0\ \cos(\frac{\pi z}{2L_{zG}})\exp(-\frac{x^2}{L_{xG}^2})\sin(\frac{2\pi t}{t_G}) & z < L_{zG} \\ 0 & z \geq L_{zG} \end{cases} \tag{34}$$

While F_0 and L_{xG} have the same values as in the previous case, t_G is now the period of the generated wave. We choose $t_G = 40$ s, which means that the maximum rate of force variation is comparable to the maximum rate in the quasi-stationary case. To allow the generator to radiate waves with this period efficiently we choose $L_{zG} = V_{AG}t_G/4$, where V_{AG} is the Alfvén velocity in the generator region.

2.6. Initial Conditions

The initial conditions for the simulation are determined from stationary kinetic theory. The boundary conditions for the temperatures and densities in this initialization are $T_M = 1$ keV and $n_M = 3 \cdot 10^5$ m^{-3} at the magnetospheric boundary, and $T_I = 1$ eV and $n_I = 1 \cdot 10^9$ m^{-3} at the ionospheric boundary. We apply an ambipolar electrostatic potential of the shape

$$\phi_{\mathrm{amb}}(z) = \begin{cases} 0 & z < 0.9L_z \\ E_{\mathrm{amb}}(0.9L_z - z) & z \geq 0.9L_z \end{cases} \tag{35}$$

where E_{amb} is a constant. Assuming Maxwellian electron distributions at the boundaries, we use the algorithm presented in *Vedin and Rönnmark* [2004] to calculate the current from kinetic theory. By adjusting the value of E_{amb} until $j_z = 0$ we determine the ambipolar potential drop, which for the boundary conditions given above is $\Delta\phi_{\mathrm{amb}} \approx 6.2$ V. We then calculate the electron density $n_0(z)$ and temperatures $T_{z0}(z)$ and $T_{\perp 0}(z)$ in the initial state with no current. The fixed background ion density n_i is determined by setting $n_i = n_0(z)$.

From the stationary kinetic model [*Vedin and Rönnmark*, 2004] used when initializing the electron fluid, we know the velocity distribution function of the electrons at all points along the field line. Given this information and the total number of simulation particles that we want to place in the system, we can load the correct number of particles in each grid cell and give them the correct velocity distribution. This particle loading procedure ensures that the moments of the particle velocity distribution are consistent with the moments in the field solver. There are two groups of electrons, magnetospheric electrons and ionospheric electrons. They are treated separately, although the moments of their velocity distributions are combined into a common variable before returned to the field solver. Note that while the ionospheric electrons are concentrated at low altitudes where the density is high, a vast majority of the magnetospheric electrons are found at high altitudes. The density of magnetospheric electrons only increases by a factor two with altitude, but the number of electrons per unit length along the diverging field lines of the flux tube increases by more than a factor 10^3. To produce statistically significant moments there must be more than $\sim 20 - 30$ magnetospheric particles in the grid cell closest to the ionosphere. This implies that there will be more than one million magnetospheric electrons in the grid cell closest to the generator boundary, and a total of about 20 million particles along one field line. Thus, to properly describe the interesting physics at lower altitudes we must include a huge number of particles in the less interesting region at high altitudes.

2.7. Boundary Conditions

During the simulation, all particles that move outside the system are removed, and new particles are injected at a rate determined by the prescribed density and temperature at the boundary. We introduce the subscript s to denote

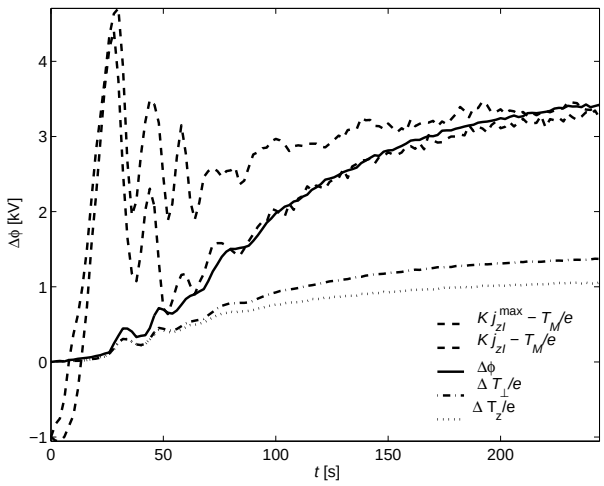

Figure 2. Time evolution of the potential drop together with the current density and the temperature perturbations scaled to kV. The fields are extracted from the simulation data at the x-value having the largest upward current density. The smaller value of current density is computed at the acceleration region (at $h \approx 5000$ km), while the larger value is the maximum value along the chosen field line. To obtain rescaled current densities comparable to the potential drop we use the current density at the ionosphere $j_{zI} = B_I/B_z j_z$, and rescale this current density according to Knight's linear current-voltage relation (38). The values of the temperature perturbations are the maximum values along the selected field line.

either magnetospheric electrons (injected at the magnetospheric boundary) or ionospheric electrons (injected at the ionospheric boundary). Assuming Maxwellian distributions, the number of particles injected at the boundary s in each time step is then given by

$$N_s^i = \Delta t N_s \sqrt{\frac{T_s}{2\pi m}} \frac{n_s/B_s}{\int n_{0s}(z)/B_z(z)dz}, \qquad (36)$$

where T_s, n_s and B_s are defined earlier with $s = M, I$, while N_s is the total number of simulation particles of group s and $n_{0s}(z)$ is the initial density profile of electrons in group s.

In the field solver the lower ionosphere is represented by a height-integrated ionospheric Pedersen conductivity, which we take to be $\Sigma_P = 10\ \Omega^{-1}$. Integrating Ohm's law and Ampere's law across the ionospheric height leads to the condition

$$E_x(L_z) = \frac{1}{\mu_0 \Sigma_P} B_y(L_z) \qquad (37)$$

at the ionospheric boundary. The perpendicular magnetic field B_y, and the current are extrapolated at the ionospheric boundary, while the density is kept constant. No ionospheric boundary condition is needed for the field-aligned electric field E_z.

Since the generator force is symmetric around the equator, we choose $\partial_z \mathsf{E_x} = \partial_z \mathsf{n} = \mathsf{E_z} = \mathsf{B} = \mathsf{j} = 0$ at the equatorial plane. An obvious consequence of these boundary conditions is that only modes with a symmetric perpendicular electric field will be included.

At the $x = \pm L_x$ boundaries we use open boundary conditions allowing perturbations to flow out of the system without reflection.

3. Results

Using the new simulation model presented in section 2 we can for the first time describe the build-up of auroral currents in presence of electron heating. The electron heating is a fundamental consequence of the auroral acceleration process, and it is essential for the build-up of the large field-aligned potential drop found above discrete auroral arcs.

This paper should be considered as a model description and will be followed by studies focusing on specific results from the model. Therefore, we will in this section only present some selected results to demonstrate that the model is properly working, and some results on monochromatic Alfvén waves complementing the results in *Vedin and Rönnmark* [2005].

3.1. Quasi-Stationary Generator

When presenting the quasi-stationary results we will use the electrostatic potential $-\partial_z \phi = E_z$, and the potential drop $\Delta\phi = \phi(z = L_z) - \phi(z = 0)$. In the stationary case, kinetic theory predicts a linear relation between the current density in the ionosphere $j_{zI} = B_I/B_z j_z$ and the potential drop $\Delta\phi$. This current-voltage relation can be written [*Knight*, 1973; *Fridman and Lemaire*, 1980]

$$j_{zI} \approx -\frac{n_M e^2}{\sqrt{2\pi m T_M}} \left(\frac{T_M}{e} + \Delta\phi \right) \equiv \frac{1}{K} \left(\frac{T_M}{e} + \Delta\phi \right). \qquad (38)$$

Figure 2 shows the time evolution of the current density, the potential drop, and the maximum temperature pertur-

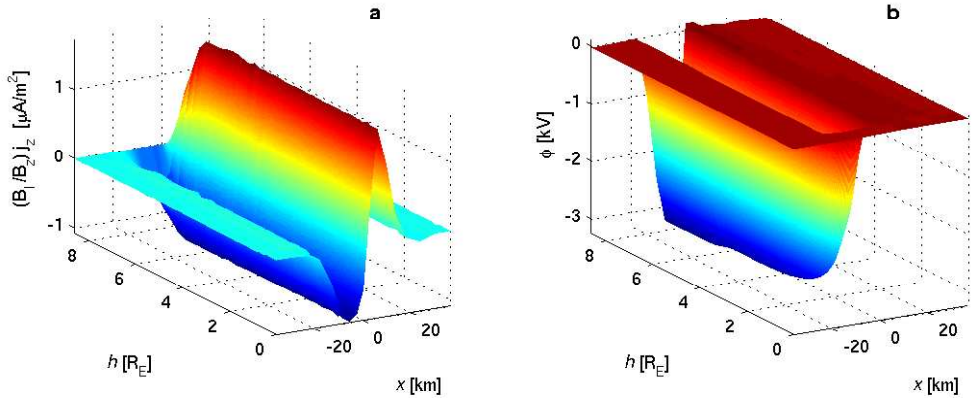

Figure 3. The quasi-stationary state of (a) the field-aligned current density mapped to the ionosphere, and (b) the electrostatic potential ϕ. The snapshots are taken 200 s after the generator was started.

bations, along the field line with the maximum upward current density. The figure contains two different current densities. The larger current $j_{zI}^{\max}$ is the maximum current along the selected field line, usually occurring about $1R_E$ below the equatorial boundary, while the other current j_{zI} is computed in the acceleration region at an altitude of $h \approx 5000$ km. Remember that both current densities are rescaled by B_I/B_z to be comparable. When these currents differ, as in the build-up phase in the figure, parts of the current is closed by an ion polarization current and a small part of the current produces a net charge density that through Gauss' law generates an electrostatic electric field. As the current continues to increase, the two currents j_{zI} and $j_{zI}^{\max}$ become equal and all the field-aligned current is closed by the perpendicular currents in the ionosphere.

Considering the early time evolution we see in Figure 2 that the current increases on the time scale of the generator (~ 10 s), while the temperatures and the potential increase on a characteristic time scale ~ 100 s. During the first 30 s of the simulation there are no significant temperature increases, and the current can grow without causing a large potential drop, as expected in an isothermal model [e.g., *Vedin and Rönnmark*, 2005]. Following the initial increase, we see a number of oscillations indicating that standing Alfvén waves are superimposed on the monotonically increasing current. However, these oscillations are strongly damped when dissipation caused by the increasing field-aligned potential drop becomes significant.

When the temperatures start to increase, the potential drop increases on the same time scale. This can be understood from the momentum equation (17e), where the temperatures balance the electric field. After more than 200 s the results approach a stationary state, where Knight's current-voltage relation is expected to hold. As indicated in Figure 2, the current density rescaled to kV using Knight's current voltage relation is then independent of altitude and similar to the potential drop in kV. However, it is interesting to notice that considering the current in the acceleration region, Knight's current-voltage relation is valid already after ∼50-100 s, although a stationary state has not been reached.

Figures 3 and 4 show some selected fields in the quasi-stationary state where Knight's current-voltage relation holds. Figure 4 shows the temperature perturbations $\Delta T_z \equiv T_z - T_{z0}$ and $\Delta T_\perp \equiv T_\perp - T_{\perp 0}$ at $t = 200$ s. Both the parallel and perpendicular temperatures are strongly enhanced in the upward current region at altitudes $\gtrsim 3000$ km. In Figure 3 the current and the field-aligned potential ϕ are presented 200 s after the simulation started. A more detailed presentation of the electric field and the temperature perturbations is given in Figure 5, where the left panel shows the fields in the upward current region and the right panel shows the fields in the downward current region. The heating of the electrons and the large acceleration almost exclusively occur in the upward current region. Actually, the heating in the downward current region is so small that it is barely above the noise level for the moments of the particle distribution. Significant electron heating observed in the return current region [e.g., *Carlson et al.*, 1998] is probably caused by wave-particle interactions, which are not included in our model.

3.2. Monochromatic Generator

The build-up of a potential drop along auroral field lines can cause reflection of shear Alfvén waves from the auroral acceleration region [*Vogt and Haerendel*, 1998; *Streltsov and Lotko*, 2003]. *Vedin and Rönnmark* [2005] demonstrated that while Alfvén waves were reflected from the ionosphere in an isothermal model, they were almost completely reflected from the acceleration region when an adiabatic model

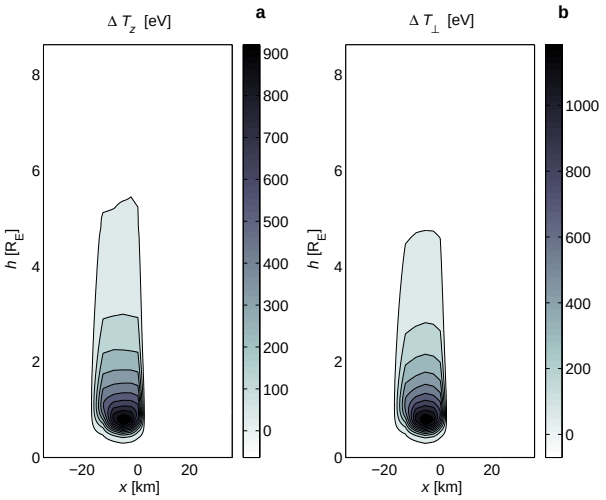

Figure 4. The quasi-stationary state of (a) the parallel temperature perturbation, and (b) the perpendicular temperature perturbation. The snapshots are taken 200 s after the generator was started.

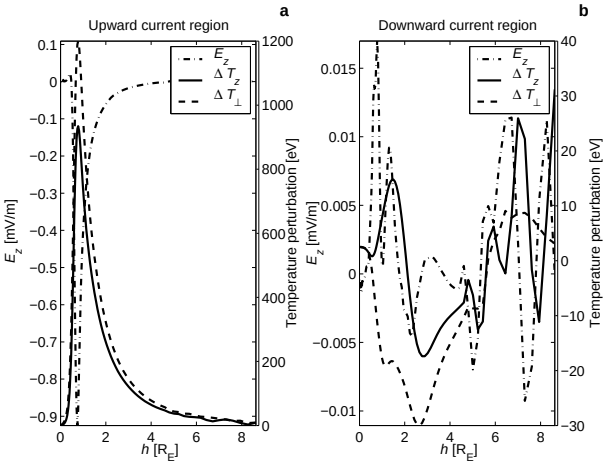

Figure 5. Plots of the electric field and the temperature perturbations 200 s after the generator was started, (a) the field line with the maximum upward current, and (b) the field line with the maximum downward current. In the downward current region the heating is barely recognizable within the noise in the moments of the particles' velocity distribution.

was assumed. The stationary kinetic model used by *Vedin and Rönnmark* [2005] could not be trusted to describe the dynamics of Alfvén waves reliably, but using the particle-fluid model we can study the effects of temperature increases on the reflection of Alfvén waves on auroral field lines.

As can be seen from Figure 2, the temperature increases lag the current increase by at least 10 s. The waves studied by *Vedin and Rönnmark* [2005] had a period of 10 s, but with the plasma parameters adopted in this study such waves hardly cause any temperature variations. Preliminary results indicate that we can make these waves create significant temperature increases in the acceleration region by reducing T_M and n_M, but here we will show the results obtained when the plasma parameters are kept constant and the wave period is increased to $t_G = 40$ s.

We concentrate on the wave fields E_x and B_y related to the shear Alfvén wave. Figure 6 shows E_x and B_y sampled

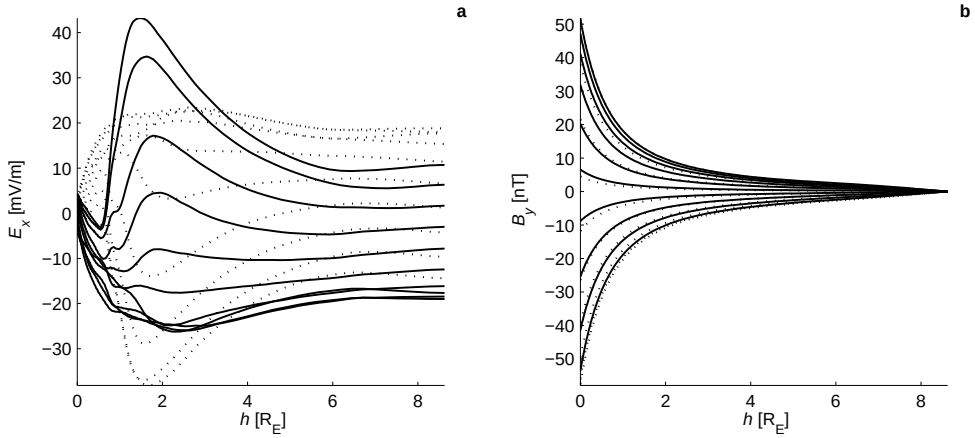

Figure 6. Plots at $x = 0$ showing the fields related to the monochromatic Alfvén waves during one wave period of $t_G = 40$ s, (a) the perpendicular electric field E_x, and (b) the perpendicular magnetic field B_y. The fields are sampled evenly 20 times during a period starting at $t = 40$ s. The first half of the cycle is shown as full lines and the second half as dotted lines. The sampling starts with the uppermost curve in both plots, and at this time ($t = 40$ s) the electron heating is large and reflection occurs at the acceleration region which results in $E_x \approx 0$ at lower altitudes.

evenly 20 times during a wave period, starting at $t = 40$ s. This figure can be compared with Figures 2 and 4 in *Vedin and Rönnmark* [2005], which show the corresponding results in the isothermal and adiabatic cases. Studying Figure 6 we see that the Alfvén waves in the particle-fluid model reflect from the ionosphere during parts of the cycle and from the acceleration region during the other parts of the cycle.

A clearer picture of how E_x and B_y at $h \approx 1.5\,\mathrm{R_E}$ vary during a wave period is shown in Figure 7. At for example $t = 50$ s, when $B_y = 0$ and the current changes direction, there will be no significant temperature enhancement. Since the temperatures are lagging they will remain low while the magnitude of the current starts to increase, and during this phase the wave is reflected from the ionosphere as in the isothermal case. A few seconds before the peak current is reached, the the magnitude of E_x suddenly increases and the phase difference between E_x and B_y is reduced. This indicates that the wave is now partially reflected by the high impedance associated with temperature increases and field-aligned currents in the acceleration region. The strong distortion of the wave form seen in Figure 7 is a striking consequence of the electron heating, but the effect is rather localized in azimuth as well as altitude. Hence, it will be difficult to observe it directly from a moving spacecraft. However, it may be possible to observe related effects under more favorable conditions, for example when higher frequency Alfvén waves are superimposed on a steady current.

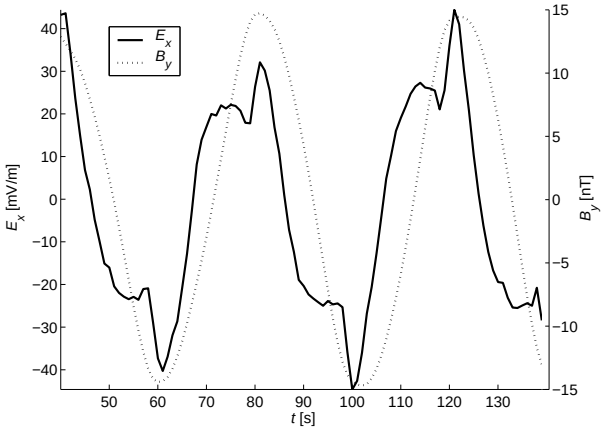

Figure 7. The time evolution of E_x and B_y at $h \approx 1.5\mathrm{R_E}$ showing 2.5 periods starting at $t = 40$ s.

4. Discussion and Conclusions

The particle-fluid model introduced in this study has some similarities to an electromagnetic PIC code, but there are also some crucial differences. In a PIC code where the field solver is tightly coupled to the particles through the charge density and current, the freedom to introduce simplifications that allow simulations of slower and larger scale processes is rather limited. The particle-fluid model described in this study separates the electrostatic interaction among the particles from the field solver. This makes the algorithm highly modular and allows different approximation to be introduced independently in the two parts of the simulation. In the model presented here, the implicit field solver includes the displacement current and the plasma frequency is reduced by the same amount in the fluid and particle parts. However, other approximation schemes are also feasible. For example, it should be possible to remove the plasma oscillations from the field solver by neglecting the displacement current without affecting the treatment of the particles much.

Earlier studies of auroral electron acceleration can roughly be placed in one of two groups [e.g., *Lysak and Song*, 2003]. One group has emphasized the electron acceleration by electrostatic field-aligned potential drops. These models are kinetic, electrostatic, and stationary. A very significant result from these studies is that the voltage that accelerates auroral electrons should be linearly related to the current. The second group has focused on shear Alfvén waves. Electron acceleration may be caused by the field-aligned electric field component of oblique shear Alfvén waves, described by fluid, electromagnetic, and dynamic models. However, although the development and refinement of the models within each of these groups has been substantial during more than two decades, it has not been possible to integrate the models into a unified, consistent theory. In particular, it has not been possible to demonstrate that a collisionless fluid model can produce the linear current-voltage relation predicted by kinetic, electrostatic theory. The results presented in this study are an important step towards a unified theory for auroral electron acceleration.

The particle-fluid model is the first dynamic model of the auroral current system that without invoking anomalous resistivity can produce large field-aligned electric fields. The key new ingredient is that electron temperature variations are properly accounted for by including particles in the simulation. This model reveals that the electron heating affects time-dependent processes, such as Alfvén wave reflection and field-line resonances. The first results presented here indicate that Alfvén waves in the presence of electron heating can be reflected both at the acceleration region and the ionosphere. Where the reflection occurs depends on the amount of heating, and the reflection can occur at different altitudes at different times during the wave cycle. Furthermore, the model also allows us to follow how shear Alfvén waves driven by a magnetospheric generator build up quasi-stationary currents and fields that are consistent with the linear current-voltage relation predicted by stationary kinetic theory.

Our results clearly demonstrate the importance of the electron temperature for the formation of field-aligned electric fields in the upward current region. The temperature increase in the vicinity of the acceleration region is mainly caused by two effects. First, as mentioned in the introduction, electron acceleration in a converging magnetic field will result in a horseshoe shaped distribution function with increased temperature. Second, the build-up of strong parallel electric fields implies that a significant part of the cold ionospheric electrons initially located in the acceleration region will be replaced by hot magnetospheric electrons. Anomalous resistivity is not needed to produce the field-aligned potential drop, although wave-particle interactions are likely to modify a number of details.

We find no evidence of significant temperature increases or field-aligned potential drops associated with the downward current. Observations [*Klumpar and Heikkila*, 1982; *Burch et al.*, 1983; *Marklund et al.*, 2001; *Johansson et al.*, 2004] of upgoing electron beams indicate that substantial potential drops exist also in the downward current region. In the absence of wave-particle interactions, the upward beams resulting from electrostatic acceleration of low energy ionospheric electrons should be essentially monoenergetic. However, such cold beams are unstable and will rapidly generate waves, which will scatter the electrons. While the energy spectrum of the downward accelerated electrons in auroral arcs usually has a clear lower cutoff, the spectrum of upgoing electron beams extends from low energies to an upper cutoff [*Carlson et al.*, 1998; *Lynch et al.*, 2002; *Andersson et al.*, 2002]. This is consistent with electrostatic acceleration combined with strong wave-particle scattering, and suggests that wave-particle interactions which are suppressed in this model play a crucial role in the downward current region.

In this first version of our model the ion density is kept fixed. This facilitates the comparison with stationary kinetic theory, and it is a reasonable approximation on short time scales. Small scale density cavities can form rather rapidly and modify the electric field in their vicinity, and on time scales of minutes the ion density may change also on larger scales. Strong outflows of ions are often seen as beams in the upward current region and conics or beams in the downward current region, and ion dynamics is probably essential for the development of fine structure in the accleration region. In our model it should be straightforward to include prescribed spatial gradients and time variations, but more work is required to develop a self-consistent description of the ion density variations.

An important property of this particle-fluid model is that it allows diagnostics of both particles and fields, which makes it easier to compare the simulation results to observations. Future studies based on this model may for example include:

1. Detailed comparisons between satellite observations of electrons in the auroral acceleration region and the electron distributions predicted by simulations.

2. The behavior of shear Alfvén waves and field line resonances, especially at lower altitudes and within the acceleration region. Results from such a study can be compared with the results from the numerous previous models [e.g., *Vogt and Haerendel*, 1998; *Fedorov et al.*, 2001; *Pilipenko et al.*, 2002; *Streltsov and Lotko*, 2003], and with observations [e.g., *Dombeck et al.*, 2005].

3. The details in the transient processes during the auroral build-up. For instance, how do the Alfvén wave oscillations seen in Figure 2 depend on the plasma properties, and what determines the lag of the electron heating?

4. Introduction of a varying ion density to study its effects on the structure of the acceleration region.

5. Other situations where field-aligned currents flow in a magnetic field configuration with large mirror ratio. In an astrophysical context, this may be common for example in the vicinity of stars and influence processes such as coronal heating and flares.

Acknowledgments. This research was conducted using the resources of High Performance Computing Center North (HPC2N), and was supported by the Swedish National Graduate School of Space Technology.

References

Andersson, L., R. E. Ergun, D. L. Newman, J. P. McFadden, C. W. Carlson, and Y.-J. Su (2002), Characteristics of parallel electric fields in the downward current region of the aurora, *Phys. Plasmas*, *9*, 3600.

Birdsall, C. K., and A. B. Langdon (1985), *Plasma physics via computer simulation*, McGraw-Hill Book Company, New York.

Burch, J. L., P. H. Reiff, and M. Sugiura (1983), Upward electron beams measured by DE-1: A primary source of dayside region-1 Birkeland currents, *Geophys. Res. Lett.*, *10*, 753–756.

Carlson, C. W., J. P. McFadden, R. E. Ergun, M. Temerin, W. Peria, F. S. Mozer, D. M. Klumpar, E. G. Shelley, W. P. Peterson, E. Moebius, R. Elphic, R. Strangeway, C. Cattell, and R. Pfaff (1998), FAST observations in the downward auroral current region: Energetic upgoing electron beams, parallel potential drops, and ion heating, *Geophys. Res. Lett.*, *25*, 2017–2020.

Cheng, C. Z., T. C. Cheng, C. A. Lin, and W. H. Tsai (1993), Magnetohydrodynamic theory of field line resonances in the magnetosphere, *J. Geophys. Res.*, *98*, 11,339–11,347.

Chiu, Y. T., and M. Schulz (1978), Self-consistent particle and parallel electrostatic field distribution in the magnetospheric-ionospheric auroral region, *J. Geophys. Res.*, *83*, 629–642.

Damiano, P. A., R. D. Sydora, and J. C. Samson (2003), Hybrid magnetohydrodynamic-kinetic model of standing shear Alfvén waves, *J. Plasma Phys.*, *69*, 277–304, doi: 10.1017/S0022377803002216.

Dombeck, J., C. Cattell, J. R. Wygant, A. Keiling, and J. Scudder (2005), Alfvén waves and Poynting flux observed simultaneously by Polar and FAST in the plasma sheet boundary layer, *J. Geophys. Res.*, *110*, A12S90, doi:10.1029/2005JA011269.

Evans, D. S. (1968), The observations of a near monoenergetic flux of auroral electrons, *J. Geophys. Res.*, *73*, 2315–2323.

Evans, D. S. (1974), Precipitating electron fluxes formed by a magnetic field aligned potential difference, *J. Geophys. Res.*, *79*, 2853–2858.

Fedorov, E., V. Pilipenko, and M. J. Engebretson (2001), ULF wave damping in the auroral acceleration region, *J. Geophys. Res.*, *106*, 6203–6212.

Fridman, M., and J. Lemaire (1980), Relationship between auroral electrons fluxes and field aligned electric potential difference, *J. Geophys. Res.*, *85*, 664–670.

Génot, V., P. Louarn, and F. Mottez (2000), Electron acceleration by Alfvén waves in density cavities, *J. Geophys. Res.*, *105*(A12), 27,611–27,620.

Génot, V., P. Louarn, and F. Mottez (2001), Fast evolving spatial structure of auroral parallel electric fields, *J. Geophys. Res.*, *106*(A12), 29,633–29,643.

Goertz, C. K., and R. W. Boswell (1979), Magnetosphere-ionosphere coupling, *J. Geophys. Res.*, *84*, 7239–7246.

Hoffman, R. A. (1993), From balloons to chemical releases–what do charged particles tell us about the auroral potential region?, in *Auroral plasma dynamics, Geophysical Monograph 80*, pp. 133–142, American Geophysical Union, Washington, DC.

Hui, C.-H., and C. E. Seyler (1992), Electron acceleration by Alfvén waves in the magnetosphere, *J. Geophys. Res.*, *97*(A4), 3953–3963.

Hull, A. J., J. W. Bonnell, F. S. Mozer, and J. D. Scudder (2003a), A statistical study of large-amplitude parallel electric fields in the upward current region of the auroral acceleration region, *J. Geophys. Res.*, *108*(A1), 1007, doi:10.1029/2001JA007540.

Hull, A. J., J. W. Bonnell, F. S. Mozer, J. D. Scudder, and C. C. Chaston (2003b), Large parallel electric fields in the upward current region of the aurora: Evidence for ambipolar effects, *J. Geophys. Res.*, *108*(A6), 1265, doi:10.1029/2002JA009682.

Johansson, T., S. Figueiredo, T. Karlsson, G. Marklund, A. Fazakerley, S. Buchert, P.-A. Lindqvist, and H. Nilsson (2004), Intense high-altitude auroral electric fields—temporal and spatial characteristics, *Ann. Geophys.*, *22*, 2485–2495.

Kletzing, C. A. (1994), Electron acceleration by kinetic Alfvén waves, *J. Geophys. Res.*, *99*, 11,095–11,103.

Klumpar, D. M., and W. J. Heikkila (1982), Electrons in the ionosphere source cone: Evidence for runaway electrons as carriers of downward Birkeland currents, *Geophys. Res. Lett.*, *9*, 873–876.

Knight, S. (1973), Parallel electric fields, *Planet. Space Sci.*, *21*, 741–750.

Lynch, K. A., J. W. Bonnell, C. W. Carlson, and W. J. Peria (2002), Return current region aurora: $E_{\parallel}$, j_z particle energization and broadband ELF wave activity, *J. Geophys. Res.*, *107*(A7), 1115, doi:10.1029/2001JA900134.

Lysak, R. L. (1985), Auroral electrodynamics with current and voltage generators, *J. Geophys. Res.*, *90*, 4178–4190.

Lysak, R. L., and C. Dum (1983), Dynamics of magnetosphere-ionosphere coupling including turbulent transport, *J. Geophys. Res.*, *88*, 365–380.

Lysak, R. L., and Y. Song (2001), A three-dimensional model of the propagation of Alfvén waves through the auroral ionosphere: First results, *Adv. Space Research*, *28*(5), 813.

Lysak, R. L., and Y. Song (2003), Kinetic theory of the Alfvén wave acceleration of auroral electrons, *J. Geophys. Res.*, *108*(A4), 8005, doi:10.1029/2002JA009406.

Marklund, G. T., N. Ivchenko, T. Karlsson, A. Fazakerley, M. Dunlop, P.-A. Lindqvist, S. Buchert, C. Owen, M. Taylor, A. Vaivads, P. Carter, M. André, and A. Balogh (2001), Temporal evolution of the electric field accelerating electrons away from the auroral ionosphere, *Nature*, *414*, 724–727.

Mizera, P. F., and J. F. Fennel (1977), Signatures of electric fields from high and low altitude particle observations, *Geophys. Res. Lett.*, *4*, 311–314.

Paschmann, G., S. Haaland, and R. Treumann (2002), Auroral plasma physics, *Space Sci. Rev.*, *103*.

Pilipenko, V., E. Fedorov, and M. J. Engebretson (2002), Alfvén resonator in the topside ionosphere beneath the auroral acceleration region, *J. Geophys. Res.*, *107*(A9), 1257, doi: 10.1029/2002JA009282.

Ramos, J. J. (2003), Dynamic evolution of the heat fluxes in a collisionless magnetized plasma, *Phys. Plasmas*, *10*(9), 3601, doi:10.1063/1.1595648.

Rönnmark, K., and M. Hamrin (2000), Auroral electron acceleration by Alfvén waves and electrostatic fields, *J. Geophys. Res.*, *105*, 25,333–25,344.

Schriver, D. (1999), Particle simulation of the auroral zone showing parallel electric fields, waves, and plasma acceleration, *J. Geophys. Res.*, *104*(A7), 14,655–14,670.

Streltsov, A. V., and W. Lotko (1999), Small-scale, "electrostatic" auroral structures and Alfvén waves, *J. Geophys. Res.*, *104*, 4411–4426.

Streltsov, A. V., and W. Lotko (2003), Reflection and absorption of Alfvénic power in the low-altitude magnetosphere, *J. Geophys. Res.*, *108*(A4), 8016, doi:10.1029/2002JA009425.

Streltsov, A. V., W. Lotko, J. R. Johnson, and C. Z. Cheng (1998), Small-scale, dispersive field line resonances in the hot magnetospheric plasma, *J. Geophys. Res.*, *103*, 26,559–26,572.

Tikhonchuk, V. T., and R. Rankin (2000), Electron kinetic effects in standing shear Alfvén waves in the dipolar magnetosphere, *Phys. Plasmas*, *7(6)*, 2630–2645.

Vedin, J., and K. Rönnmark (2004), A linear auroral current-voltage relation in fluid theory, *Ann. Geophys.*, *22*, 1719–1728.

Vedin, J., and K. Rönnmark (2005), Electron pressure effects on driven auroral Alfvén waves, *J. Geophys. Res.*, *110*, A01214, doi:10.1029/2004JA010610.

Vogt, J., and G. Haerendel (1998), Reflection and transmission of Alfvén waves at the auroral acceleration region, *Geophys. Res. Lett.*, *25*, 277–280.

K. Rönnmark and J. Vedin, Department of Physics, Umeå University, SE–901 87 Umeå, Sweden.
(email: kjell.ronnmark@space.umu.se; jorgen.vedin@space.umu.se)